Additive Manufacturing 29 (2019) 100819

Contents lists available at ScienceDirect

Additive Manufacturing

journal homepage: www.elsevier.com/locate/addma

Full Length Article

The m^4 3D printer: A multi-material multi-method additive manufacturing platform for future 3D printed structures

Devin J. Roach, Craig M. Hamel, Conner K. Dunn, Marshall V. Johnson, Xiao Kuang, H. Jerry Qi*

G.W.W. School of Mechanical Engineering, Georgia Institute of Technology, Atlanta, GA 30332, United States

ARTICLE INFO

Keywords:
Hybrid 3D printing
Multimaterial 3D printing
4D printing
Flexible electronics
Soft robotics

ABSTRACT

The advent of additive manufacturing (AM), also often referred to as 3D printing, has enabled the rapid production of parts with complex geometries that are either labor-intensive or unrealizable by traditional manufacturing methods. Many existing 3D printing technologies, however, only allow one material to be printed at one time, while many applications require the integration of different materials, which sometimes cannot be printed by one AM technology. In this paper, a novel multi-material multi-method (m^4) 3D printer comprised of multiple AM technologies is presented as a solution to the current limitations. This printer fosters the advancement of AM by combining materials traditionally unable to be printed concurrently while adding functionality to printed parts. The m^4 3D printer integrates four AM technologies and two complementary technologies onto one single platform, including inkjet (IJ), fused filament fabrication (FFF), direct ink writing (DIW), and aerosol jetting (AJ), along with robotic arms for pick-and-place (PnP) and photonic curing for intense pulsed light (IPL) sintering. The integration of these AM technologies and PnP into a single platform allows for rapid fabrication of complex devices, providing a wide range of functionalities with applications ranging from soft robotics and flexible electronics to medical devices.

1. Introduction

Additive manufacturing (AM), also often referred to as 3D Printing, can enable the rapid production of parts consisting of complex geometries that are labor-intensive or even unrealizable by traditional manufacturing methods. This concept was introduced in the 1980s [1] and gained much attention from hobbyists and industries alike. Today, manufacturing sectors in aerospace, automotive, and electronics are beginning to take notice of AM's power for rapid prototyping, with AM representing a $7 billion industry in 2017 [2]. The AM market achieved a 21% growth in 2017 and it is projected that by 2023 the market could be worth $33 billion [3]. Industries also reported an average of a 60% increase in their budget for AM technologies between 2016 and 2017 [4]. More recently, industries have turned to AM to produce functional and end-use parts with real applications. NASA, for example, 3D printed a fuel injector, reducing the number of manufacturing steps from 163 to two [5]. Boeing first used AM to fabricate a nadir surface mounted optical bench in the SES-15 spacecraft and is now delivering nearly 1000 AM parts to flight programs throughout their fleet [6]. The materials that can be used for AM have also expanded significantly. Traditional AM technologies started with printing thermoplastics and photopolymers, but today, many new approaches have been developed to print materials such as metals [7–9], conductive inks [10–13], functional polymers [14–18], and ceramics [19–21].

Currently there are many different 3D printing techniques, which can be classified into seven categories defined by an ASTM standard [22]. These include binder jetting, material extrusion, material jetting, powder bed fusion, sheet lamination, and vat photo-polymerization. Material extrusion and material jetting (including fused filament fabrication (FFF), direct ink write (DIW), and inkjet (IJ)) have the common feature of depositing material in an as-needed and controlled manner onto the building platform. To fabricate a 3D object using FFF, filament of a thermoplastic polymer is fed into a print-head where it is melted and extruded to form a specified 2D geometry, which is then deposited in a layer-by-layer fashion to form a 3D part. DIW uses a similar strategy, however, the raw material is typically liquid resin with a high enough viscosity to hold the 3D shape after extrusion. IJ works very similarly to an office desktop printer and uses an array of small print-heads to deposit droplets of photopolymer ink. After a layer of ink is jetted, it is irradiated by UV light for curing and this process is repeated to form a 3D object. Both FFF and DIW are line-based methods and typically use G-code directly for printing. On the other hand, IJ uses G-code to control the motion stage and a bitmap image to control the ink deposition. The remaining 3D printing methods, such as powder bed

* Corresponding author.
E-mail address: qih@me.gatech.edu (H.J. Qi).

https://doi.org/10.1016/j.addma.2019.100819
Received 13 February 2019; Received in revised form 21 June 2019; Accepted 31 July 2019
Available online 02 August 2019

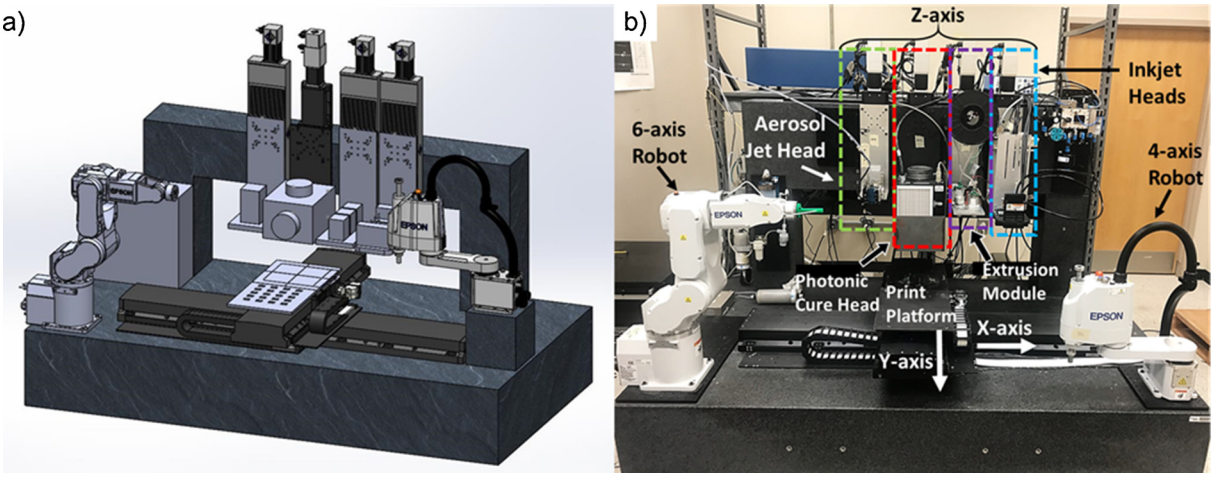

Fig. 1. a) CAD schematic of the m^4 hybrid 3D printer. b) A photograph of the assembled printer with each printhead, robot, and motion axis labeled.

fusion and vat photo-polymerization, have the common feature of creating a 3D structure from a vat of raw material such as a powder bed or liquid resin container. Typically, the raw material is sintered or crosslinked via an energy source such as a UV light, heat source, or laser beam. The most commonly recognized 3D printing methods relying on this technique are stereolithography (SL), selective laser sintering (SLS), and digital light processing (DLP). The rich variety in 3D printing technologies reflects the tremendous varieties in materials and their associated composition, molecular structures, melting temperatures, types of phase transitions, and other material properties.

Previously, 3D printing has been used as a prototyping technique to fabricate early-stage products which were primarily used for visual inspection or temporary functionality. However, as 3D printing moves into the future, it is highly desirable to print multiple materials in the same printing job for enhanced visual inspection and increased functionality. Multiple material printing can enable enhanced properties like controllable material anisotropy, which can be critical for functional devices such as those requiring surface compliance yet high load capacity [23]. In addition, printing multiple materials with distinct properties such as shape memory polymers or conducting polymers can further enhance functionality to create smart grippers or crawling robots [24,25]. Initial efforts towards a hybrid additive manufacturing platform were aimed at printing multiple materials using a single printing method. Polyjet technology, for example, utilizes multiple inkjet printheads to jet different photopolymer inks to fabricate structures composed of different materials. The Connex printer series, developed by Stratasys, utilizes Polyjet technology and has been used extensively in research labs and industry for a myriad of applications such as bio-inspired mechanics studies [26–28], self-assembly, direct 4D printing [29], and digital shape memory polymers [30]. By combining materials with a wide range of mechanical properties and high-resolution printing, digital materials can be made such that the material properties may vary greatly from point to point. FFF structures utilizing multiple materials have also been reported [31] but these structures typically suffer from poor interfacial adhesion. Lastly, multi-material SL printing has been reported [32,33] but multiple resin vats are required as well as cleaning and other post-processing operations when switching between materials. In recent years, a few notable efforts towards AM hybridization have been reported by incorporating two of the printing methods listed above to create a single 3D part. SL and DIW have been combined for uninterrupted electronics fabrication [34] while FFF and DIW have been combined for embedded electronics fabrication. A notable example of the latter is the commercial product of Voxel8 (Voxel8, Sommerville MA, USA), representing a major milestone in hybrid manufacturing. The Keck Center at UT El Paso has recently started to incorporate robotic assistance into an AM process [35] which greatly reduces the amount of interruptions in the manufacturing procedure. Such a methodology, using robotic placement tools together with other prevailing 3D printing methods, was also explored by other groups [24,36]. Also, some design considerations and principles were attempted and discussed [37,38]. These efforts demonstrate the potentials and the importance of integrating printing technologies to create functional devices. Incorporating many methodologies into a single 3D printing platform would introduce a novel design space for functional devices [39].

In this paper, we present our methodology for building a multi-material multi-method (m^4) 3D printer that integrates a wide variety of deposition-based AM technologies. The m^4 3D printer utilizes common AM technologies including: IJ, FFF, DIW, and aerosol jetting (AJ) along with complementary robotic pick-and-place (PNP) and intense pulsed light (IPL) photonic curing. The integration of these AM technologies and PNP into a single platform enables parts to be fabricated by using multiple materials and AM technologies as well as non-printable components which may be too difficult, expensive, or even impossible to print by using current AM paradigms. We will further demonstrate how the m^4 3D printer can foster the advancement of 3D printing by combining materials traditionally impossible to be printed concurrently by adding novel functionalities to 3D printed parts. Devices including embedded electronics, sensors, soft robotics, and customizable medical devices could be more easily manufactured for on-site surgical, battlefield, or space applications.

2. Platform overview

The AM technologies in the m^4 3D printer are deposition-based methods, as they are self-contained and did not require resin vats or powder beds. Although there might be needs to include vat-based methods, our current choice had the advantage of selective material placing without the need for extra cleaning after material deposition. In addition, as shown below, this allows us to shuttle the printed part between different printing methods. In total, the integrated system contains seven printheads from four different AM technologies (two FFF heads, two DIW heads, two IJ heads, and one AJ head), two in-situ curing modules (photonic and UV), and two robotic arms for PnP and conformal printing. Fig. 1a shows a CAD schematic of the printer and Fig. 1b shows a photo of the assembled printer.

2.1. Hardware

Due to the complexity of integrating 7 printheads, curing modules, and robotic arms into one platform, five motion stages (one x-y motion stage and four z-motion stages) are used (Aerotech Inc., Pittsburgh, PA,

USA). All printheads and curing modules are mounted on the z-motion stages while the print bed sits on the x-y motion stage to shuttle the part between different printheads. The x-y motion stage has a large working envelope of 1 m x 0.5 m, a local accuracy of ± 3 µm, repeatability of ± 1 µm, and a maximum velocity of 1.0 m/s. The z-axis motion stages achieve the layer-by-layer deposition. Each z-axis has 0.25 m of vertical travel, an accuracy of ± 1 µm, a repeatability of ± 0.5 µm, and a maximum velocity of 0.7 m/s. The printing modules fixated to the four z-axis stages include: Aerosol Jetting, Photonic Curing, Extrusion (DIW and FFF), and IJ modules as shown in Fig. 1b. To find these specifications tabulated the readers are referred to Table S1 in the Supplementary Materials (SM).

2.1.1. Aerosol jetting module

The Aerosol Jetting module is an Optomec Print Engine (AJ 5X System, Optomec Inc., Albuquerque, New Mexico, USA) with a pneumatic atomizer, capable of printing materials including, but not limited to, conductors, dielectrics, ceramics and adhesives, all with fine feature sizes (line width of 10 s–100 microns).

2.1.2. Photonic curing module

The photonic curing module is a Xenon flash lamp (model RC-847, Xenon Corp., USA) which emits a broad-spectrum light, 240–800 nm, capable of irradiating 19.44 J/pulse at 100 Hz. The photonic curing system can be used to cure printed inks, including silver nanoparticle-based ink during the printing process, as studied in our previous works [40]. This module eliminates the long curing times required in standard ovens (~30 min) [11] and provides a rapid, uninterrupted printing and curing process that can occur on the m^4 3D printer's motion stage.

2.1.3. Extrusion module

The extrusion module consists of two AM processes: FFF and DIW. Two commercial FFF printheads purchased from Prusa3D (Prague, Czech Republic) are mounted to the extrusion module. The DIW uses two syringes, controlled by one precision pneumatic pressure regulator (UltimusV, Nordson EFD, East Providence, RI, USA), which is accurate up to 0.1 psi and has a maximum pressure output of 100 psi. The syringes are mounted in metal sleeves with embedded heaters, which are used for printing highly viscous resins.

2.1.4. Inkjet module

The photopolymer IJ module consists of two Xaar 1003 (Xaar Plc, United Kingdom) piezoelectric drop-on-demand printheads, a FE300 LED UV lamp (Phoseon, Hillsboro, OR) for curing, a Hydra ink supply system from Xaar, and the corresponding control electronics.

2.1.5. Robotic arms

Two robotic arms are mounted for PnP applications, conformal printing processes, or in-situ measurement devices. On the left side is an Epson 6-axis robotic manipulator (C4, Epson Inc., Nagano, Japan) and on the right is an Epson 4-axis robotic manipulator (G3, Epson Inc., Nagano, Japan).

2.2. Electrical control and communication

The m^4 printer is controlled by one desktop computer that interfaces with the m^4 printer. All motions involved in the printing process are controlled by either the dedicated Aerotech A3200 motion controller or the robotic controller. The motions in all six linear axes are controlled independently, allowing coordinated motion commands between the multiple motion stages. The robot controller controls all pre-programed pick and place routines for the 4 and 6-axis robotic arms. To synchronize the motion stages, material deposition, and robot motion, an in-house software coded in Python was developed for the m^4 3D printer. The motion commands for the six linear motion stages are supplied via traditional G-code while the robot movements are delegated by the controller's interface language.

2.3. Hybridization of 3D printing methodologies

2.3.1. Coordinate transformations

The primary challenge encountered when integrating multiple printing technologies was that each technique has its own unique communication language and independent coordinate system. Extrusion based single nozzle 3D printing techniques (such as FFF and DIW) typically rely on G-code, a point-to-point printing scheme, whose toolpath is generated from cross-sectional slices of a solid model. Inkjet 3D printing, on the other hand, is an application that can print a single layer in a few discrete movements by utilizing an array of piezoelectric nozzles to deposit build material. Bitmap images are typically used to represent a single layer of the designed part and are thus printed accordingly. Therefore, printing with multiple printheads and techniques presents the need for transitioning between materials and their deposition methods (G-code or bitmap) while maintaining accurate positioning and printing resolution in each module. To reliably switch between different printheads and keep accurate positioning, kinematic

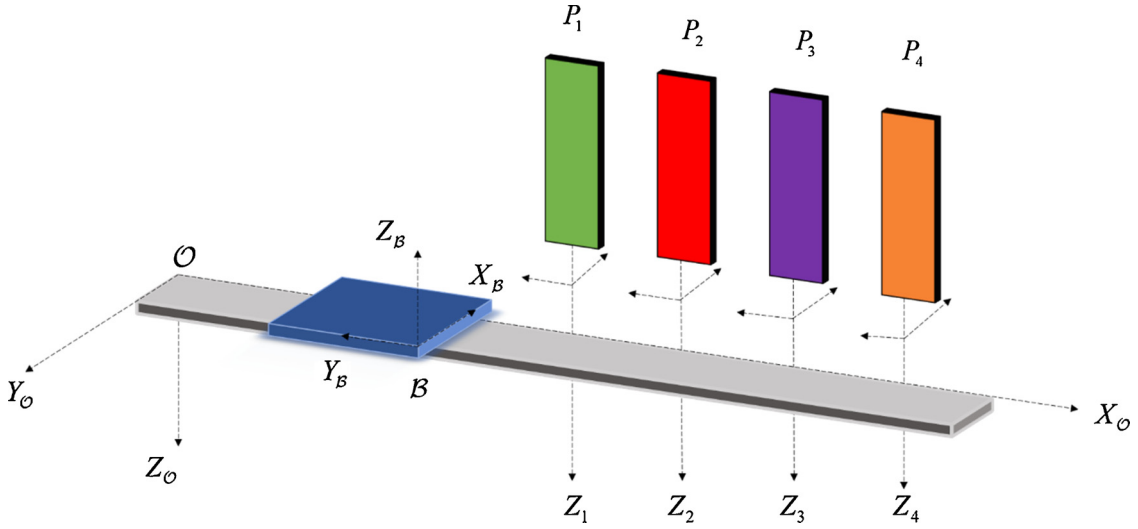

Fig. 2. Schematic of the individual coordinate systems for each print module as well as the local coordinate system of the print bed and the associated global coordinate system of the m^4 3D printer.

transformations must be developed and applied to the generated printing coordinates, as shown in Fig. 2. The generated executable G-code provides a toolpath in a local coordinate frame, $\mathcal{B}$, on the printing platform. These coordinates cannot be directly used, as the motion of the m^4 printer is dictated by the motion controller and its respective coordinate system. For the G-code coordinates to be used to move between different printheads, denoted by P_i, transformation matrices must be derived which can represent the G-code with respect to the printhead being used. First, a rotation matrix is defined to represent the rotation of a general frame, $\mathcal{B}$, with respect to the origin frame, O, of the XY motion stage, which consists of a 180° rotation about X_O and a 90° rotation about Z_O:

$$ {}^{O}_{\mathcal{B}}R = R_{Z_O}(90°)R_{Y_O}(0°)R_{X_O}(180°) = \begin{bmatrix} 0 & 1 & 0 \\ 1 & 0 & 0 \\ 0 & 0 & -1 \end{bmatrix} \tag{1} $$

After rotation, the general frame $\mathcal{B}$ only differs from frame O by a single translation which is dependent on the printhead being used, denoted by i, and the offsets associated with the particular printhead, X_i, Y_i, and Z_i, that places the origin of frame $\mathcal{B}$ at the point of the printhead. This point can be expressed by the following column vector

$$ {}^{\mathcal{O}}P_i^{\mathcal{B}} = \begin{bmatrix} X_i \\ Y_i \\ Z_i \end{bmatrix} \tag{2} $$

Any coordinate in the G-code can be described in terms of frame B with a simple vector, ${}^{B}G$, from the origin of $\mathcal{B}$,

$$ \mathcal{B}_G = \begin{bmatrix} X \\ Y \\ Z \end{bmatrix} \tag{3} $$

where X, Y, and Z are the coordinates from the G-code. Finally, by combining the rotation and translation matrices, any generated point in G-code, G, can now be represented in the motion controller's coordinates for the respective printhead, i, as ${}^{\mathcal{O}}G^i$ and defined through the block matrix equation as follows:

$$ \begin{bmatrix} O_{G^i} \\ 1 \end{bmatrix} = \begin{bmatrix} {}^{O}_{\mathcal{B}}R & {}^{O}P_i^{\mathcal{B}} \\ 0 \;\; 0 \;\; 0 & 1 \end{bmatrix} \begin{bmatrix} \mathcal{B}_G \\ 1 \end{bmatrix} \tag{4} $$

2.3.2. Printer software

To develop a printing software capable of combining each component of the m^4 3D printer into a unified program for printing, a highly complex algorithm, or work-flow must be imagined. Therefore, a flow chart was developed to visualize the printer work-flow. Fig. 3 shows a schematic of the m^4 3D printer's generalized work-flow. The work-flow was coded into Python and a user-friendly user interface (UI) printer software was developed to assist users and can be seen in the SM (Fig. S1). Using the UI, the user may input the G-code file generated by the slicing software; choose which printing techniques they wish to use; prescribe printing parameters such as speed, dwell time, or layer height; process, or translate, the G-code; and export the G-code for use in the Aerotech motion composer UI.

2.4. Materials

The m^4 hybrid 3D printer allows a wide array of materials for multi-material 3D printed parts. In this paper, the following materials were used for demonstration purposes.

2.4.1. Soft elastomer resin

The soft elastomer resin developed by Kuang, et al. [41] was used for DIW printing. Aliphatic urethane diacrylate (AUD) Ebecryl 8413 and Ebecryl 8804 were provided by Allnex USA Inc (Alpharetta, GA, USA). N-butyl acrylate, polycaprolactone (PCL, Mn = 70,000 ~ 90,000), fumed SiO_2 powder (0.2-0.3 μm particle) and glycidyl methacrylate (GMA) were purchased from Sigma-Aldrich (St. Louis, MO, USA) and used as received without further purification. The soft elastomer polymer resin was prepared by dissolving 0.8 wt % of PCL in n-butyl acrylate (BA)/ Ebecryl 8413 (1/1, wt/wt). Then 5 wt% of fumed SiO2 was gradually added into the above mixture and stirred manually until a transparent blend was obtained. Finally, 0.8 wt % of phenylbis(2,4,6-trimethylbenzoyl)phosphine oxide (Irgacure 819) was added to the total mass. The mixture was then poured into a syringe for DIW printing and centrifuged to remove air bubbles at 3500 rpm for 15 min. After printing, the elastomer resin was UV cured.

2.4.2. Conductive ink

The silver nanoparticle-based conductive ink (DuPont ME603) used in this study was purchased from DuPont Inc. (Wilminton, DE, USA). It has a solid content of 49–53%, a viscosity of 25–50 cP, and sheet resistivity of 200 mΩ sq^{-1} mil^{-1} after photonic curing. Previously, Mu, et al. determined the optimal 3D printing and photonic curing parameters which will be used in this study [40]. Five-cycle sintering with 8 s light exposure and 15 s cooling time at a distance of 39 mm from the sample was used.

2.4.3. Other materials

The inkjet material used in this study was a photocurable acrylate-based polymer (SunJet DIC Inkjet Solutions, Amelia, OH, USA). The material used for FFF is a 1.75 mm diameter spool of raw, green ABS material acquired from MakerBot Industries (Brooklyn, NY, USA). A 50 W chip LED was used as a light source in one of the demonstrations and was purchased from LOHAS LED Lighting (Chicago, Illinois, USA).

3. Results and discussions

In the following section we demonstrate the capabilities of the m^4 3D printer to produce multi-material functional devices. Each example utilizes a different combination of the printing, curing, and PNP modules to showcase the wide versatility of the m^4 3D printing platform and the potential applications of hybrid AM to various emerging technological paradigms. Previously, the m^4 3D printer was used to print a reversible shape changing smart material called liquid crystal elastomer (LCE), demonstrating multi-material smart structures without introducing the m^4 printer [42]. In addition, the m^4 3D printer was used to print a renewable cellulose nanocrystal (CNC)-based support material in conjunction with other materials to create complex structures which require support in 3D space [43]. Therefore, printing LCE and CNC-based support material is not introduced in this paper. Dimensional accuracy of the printed structures is another aspect of the following results that should be addressed. In principle, the dimensional accuracy of the printed structures depends on the specific structure, therefore it was not a primary focus of this paper; instead, the capability of printing functional structures was deemed more important in this scope. In the following, first, multi-material structures were fabricated using both IJ and DIW. Next, a soft pneumatic actuator made of two materials using DIW and IJ was demonstrated, which greatly simplifies the traditional techniques for making such devices. Third, a stretchable electronic device was fabricated using the same materials, but now including DIW printed conductive traces. Next, vertical interconnect access, or VIA, circuits were fabricated representing the first 3D printed VIA-based circuit. Lastly, an embedded electronic device was fabricated utilizing FFF for a casing, DIW for conductive traces, and PNP of a LED light.

3.1. Multi-material structures

By incorporating multiple printing methodologies into the same platform, accurately depositing multiple materials with a wide range of mechanical properties can be used to fabricate unique structures which can have varying material properties in 3D space. In addition, multi-material printing provides the advantage of layer-level integration into

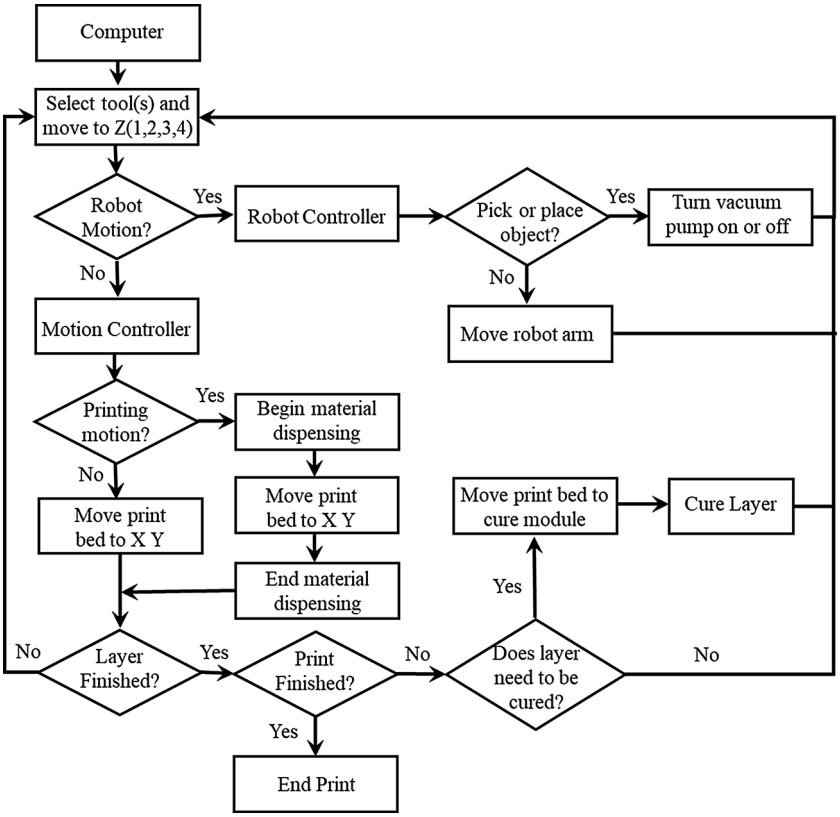

Fig. 3. General algorithm, or work-flow, coded into Python to develop the printer software.

a single part.

3.1.1. Multi-material 3D printed wheel

As a preliminary multi-material demonstration, a race car wheel was 3D printed with a soft outer tire to hold air and a rigid inner wheel serving as a structural support. Here, the tire was made from the DIW printed soft elastomer and the wheel was made from the IJ-printed photopolymer. A primary challenge encountered when attempting to use of two different methodologies for printing was the difference in resolution, especially in the vertical direction. A discussion on solving this challenge can be found in Section 3.5.1 where it was determined that eight layers of IJ was equal to one layer of DIW. Using this strategy, DIW and IJ were alternated to create the 3D wheel seen in Fig. 4a. After printing, the soft tire can deform to absorb load while the wheel remains rigid to carry load. A compressive force vs. displacement plot to simulate the loading the tire would experience if it were supporting a car is shown in Fig. 4b.

3.1.2. Multi-material interface study

One of the primary advantages garnered by m^4 printing is the precise placement of a wide range of materials in 3D space. Here, we studied the interfacial properties of three different interface shapes between the IJ photopolymer and the DIW elastomer materials. We demonstrate a blunt interface; a buzzsaw interface, which varies the interface in the x–y plane; and a lapped interface which varies the interface in the z-plane. The resulting interface shapes are shown in Fig. 4c. The samples were tested in tension using a Dynamic Mechanical Analysis (DMA) tester (Model Q800, TA Instruments, New Castle, DE, USA) using a preload force of 0.1 N and a strain rate of 0.3 mm/s. The aim of this study is to show that there is high interfacial bonding between the photopolymer and elastomer materials. Here, our printed structures can handle large deformations before failure, achieving strains of up to 350%. Undoubtedly, under tension, the strength of the multi-material samples is dictated by the interfacial failure strength and may not be suitable for all applications. The individual stress vs. strain behaviour of the DIW elastomer and the IJ photopolymer are shown in Fig. S2 in the SM. Upon failure, three distinct failure modes can be observed in Fig. 4d, with the corresponding stress vs. strain curves shown in Fig. 4e. Interestingly, the blunt interface can sustain much larger stresses and strains; twice as large as those with buzzsaw or lap interfaces. Overall, the interface between the DIW and IJ printed parts were very strong. This was partially because the inks used in our DIW and IJ methods were both photocurable, acrylate-based polymers, which admitted good compatibility, and is discussed further in Section 3.5.2. The integration of the dual-method printed portions were at the layer level, instead of at part level (i.e. printing one part after the other) which also allowed for the formation of a better interface.

3.2. Multi-material soft pneumatic actuators

Soft robotics was traditionally a term used to describe robots with ridged links and mechanically compliant joints having variable stiffness. Recently the area of soft robotics has shifted from rigid links to bioinspired continuum robots that are “inherently compliant and exhibit large strains in normal operations” [44,45]. Much work has been put into this area, but fabrication techniques for soft robots are still constrained by time-consuming and labor-intensive fabrication processes. Typically, they involve the formation of complex, multi-piece molds made by either 3D printing or traditional techniques such as embedded casting or soft lithography; processes which can take up to 3 h [46] 3D printing has enabled the ability to easily print complex mold geometries that improve the fabrication process, but the potential to use 3D printing to completely print soft robots becomes more attractive and time efficient. Here, a completely 3D printed soft pneumatic actuator is presented, based on the design of the previous work by Mosadegh, et al. [47]. The design of the soft actuator and a schematic of the working principle are illustrated in Fig. 5a. The actuator consisted of a layered structure with an extensible top layer and a flexible,

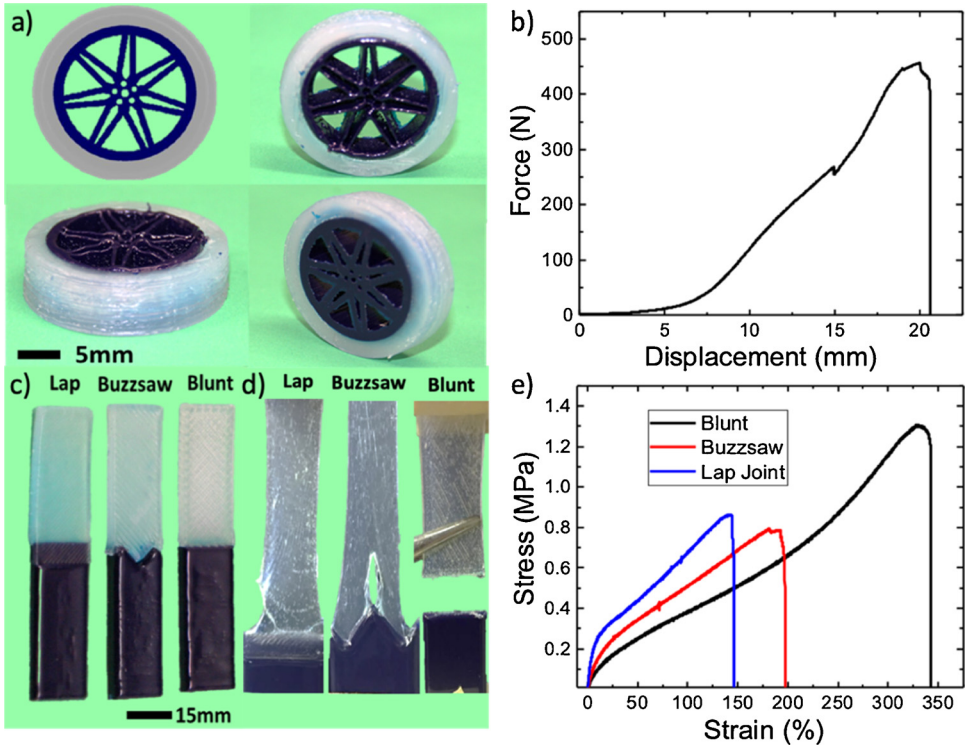

Fig. 4. (a) m^4 3D printed wheel with a DIW-printed soft elastomer tire which holds air and an inkjet-printed rigid rim to carry load. (b) Force vs. displacement curve of the tire under compression simulating a car load. (c) Different designs for an interface between stiff photopolymer material and soft elastomer material. (d) Failure locations for each interface design under tension. (e) The resulting stress vs. strain response of each sample.

inextensible bottom layer. Between the top and bottom layers were hollow chambers which could be pressurized causing expansion of the top, extensible layer. The subsequent bending deformation was a result of the difference in compliance between the two materials [47]. The actuator was printed by combining the IJ and DIW printing methods to print the same photopolymer and elastomer material used in previous demonstrations. The photopolymer ink acted as the inextensible material that enabled the bending and the DIW elastomer was the extensible material used for the remainder of the structure. The actuator was printed in a layer-by-layer fashion, switching between IJ and DIW printing heads. A top view and bottom view of the printed actuator could be seen in Fig. 5b as well as a schematic of the pneumatics used for actuation. After printing, a syringe was inserted into the printed inlet hole to supply the pressure as seen in Fig. 5c. The pressure switch was then turned on and a 20 psi pressure was applied to inflate the hollow inner cavities to induce bending, as seen in Fig. 5d. The soft material expanded but was restricted by the stiff inkjet layer on the bottom of the soft actuator causing bending toward the inextensible material. After turning the pressure switch off, the actuator rapidly returned to its initial configuration. Bending actuation of the soft actuator took around 0.5 s while the returning actuation took 0.25 s. Previously, the fabrication of multi-material elastomer-based pneumatic actuators took around 3 h [46] plus the separate fabrication of molds, whereas the full fabrication process of the actuator shown in Fig. 5 took around 5 min. A video of the m^4 3D printing and subsequent activation of the soft actuator can be seen in the SM (video 1).

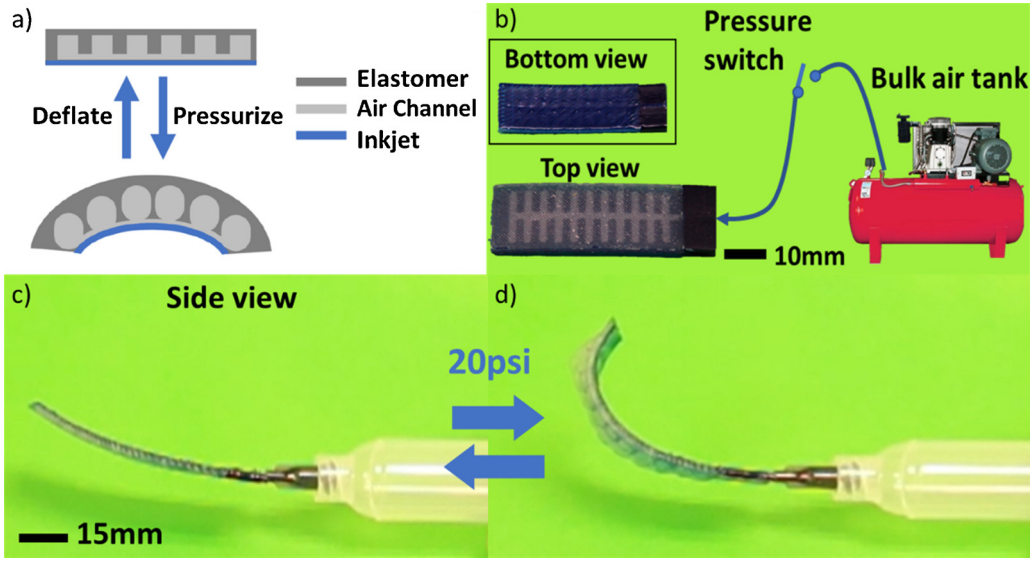

Fig. 5. a) Schematic of the working principle behind the soft pneumatic actuator. b) Top and bottom view of the soft actuator with a schematic showing the flow of air from the bulk air tank regulated by a pressure switch. c) Side view of the soft actuator when no pressure is applied and d) when a 20 psi pressure is applied.

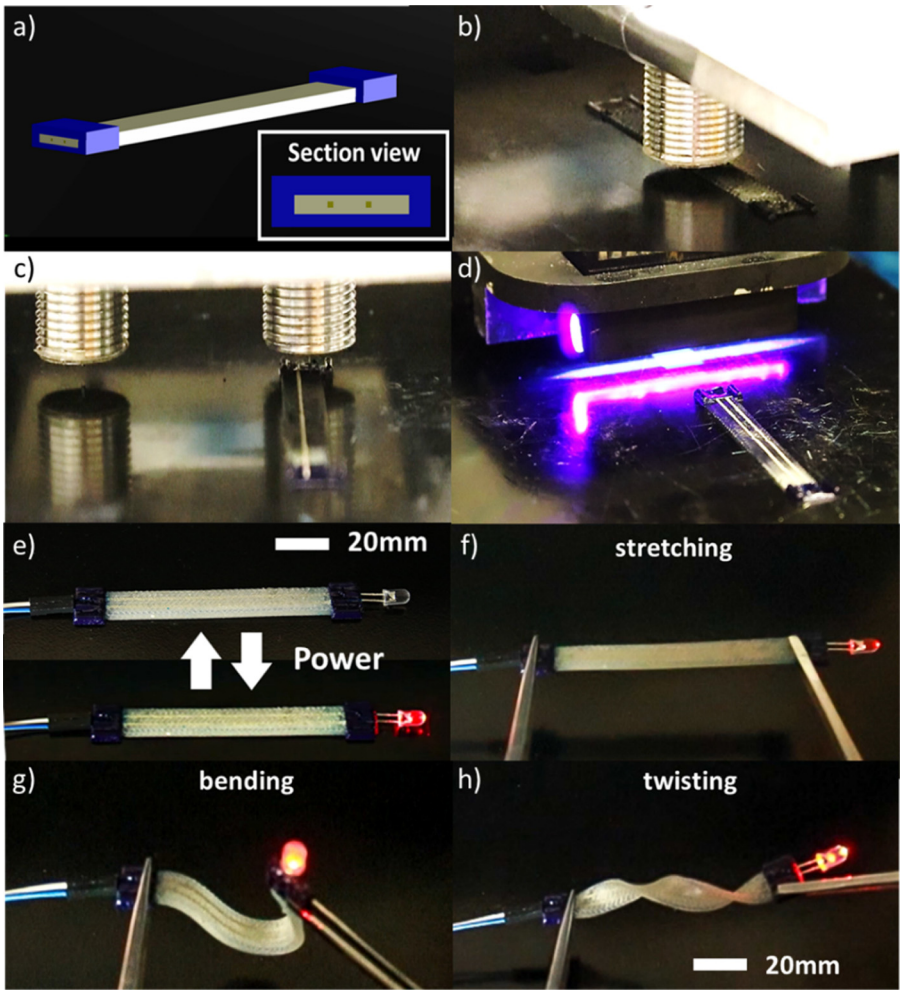

Fig. 6. a) Schematic of the stretchable light ribbon with a section view showing the blue inkjet casing, the gray stretchable elastomer, and the silver conductive lines. b) The first layer of elastomer being DIW printed between the two inkjet printed ends of the light ribbon. c) DIW printing of the conductive lines. d) Inkjet printing to encase the light ribbon's electrical lines and provide rigid support for the electrical components. e) The as-printed stretchable light ribbon with the LED and a power source plugged in to illuminate the LED. f) Stretching, g) bending, and h) twisting of the LED light ribbon while the LED stays illuminated. (For interpretation of the references to colour in this figure legend, the reader is referred to the web version of this article).

3.3. Printed electronics

3.3.1. Stretchable, multi-material light ribbon

The combined capabilities of the DIW module to print a soft elastomeric material and a stretchable silver conducting ink impart the capability of fabricating stretchable and foldable electronics within a single platform during an uninterrupted printing process. Non-flexible components added after printing such as LED lights, resistors, integrated circuits (ICs), or wires however cannot be stretched or folded and may cause the electronics to lose functionality. Therefore, IJ printing of a rigid photopolymer is advantageous for encapsulating the non-flexible components to ensure circuit functionality during stretching and folding. A schematic of a stretchable light ribbon is shown below in Fig. 6a with a section view showing the blue inkjet casing, the gray stretchable elastomer, and the silver conductive lines. Screenshots of the printing process are shown below in Fig. 6b–d (SM video 2). First, the photopolymer is IJ printed and the stretchable elastomer is DIW printed and UV-cured (Fig. 6b). Next, the conductive silver ink is DIW printed to form a conductive trace to power the LED (Fig. 6c). The silver ink is then directly cured using the Xenon photonic curing module and encapsulated with a subsequent layer of soft elastomer and photopolymer material (Fig. 6d). Wires were then plugged into one side of the conductive traces while an LED light was plugged into the other side. By supplying power, the light was illuminated (Fig. 6e). The light ribbon could then be stretched (Fig. 6f), bent (Fig. 6g), twisted (Fig. 6h) and further manipulated (SM video 3) while maintaining electrical contact to keep the LED illuminated. Indeed, the printed and sintered silver ink will have a lower conductivity than bulk silver. The sheet resistance of bulk silver is approximately 50 $m\Omega/sq^{-1}$ mil^{-1} [48] whereas the silver ink has a sheet resistance of 200 $m\Omega/sq^{-1}$ mil^{-1}. This will limit the potential applications of the printed silver ink; however, this limitation can be overcome when better conductive inks are developed. In addition, many applications such as sensors or antenna do not require very high conductivity and thus our method can be acceptable. 3D printing of stretchable electronics with rigid interfaces for non-stretchable components can find uses for electronics found in wearables, underwater, or space applications.

3.3.2. 3D printed VIA

Current approaches to print multi-layer printed circuit boards (PCBs) require many complex processing strategies. In addition, to print vertical interconnect access (or VIAs) between layers, drilling or laser-cutting as well as filling processes are required. The fabrication of typical VIA-based electronic circuits is also time-consuming; with a standard, multi-hole VIA circuit requiring up to 2 h to complete. To solve this issue, we utilized multi-material layer-by-layer printing to print a vertical conductive line and demonstrate the rapid m^4 3D printing of a VIA-based circuit. In this demonstration, a VIA conductive trace was used to illuminate an LED. A schematic of the design used to print the VIA is shown in Fig. 7a. For the first layer, horizontal conductive lines were printed on an inkjet substrate. For the subsequent layers, conductive material was DIW printed in the empty locations within the inkjet structure to build the vertical conductive trace. To solve this issue, each layer of conductive ink was partially cured by evaporating the solvent using the heat generated from a heated printing platform (˜50 °C). The conductive VIA lines were further cured and

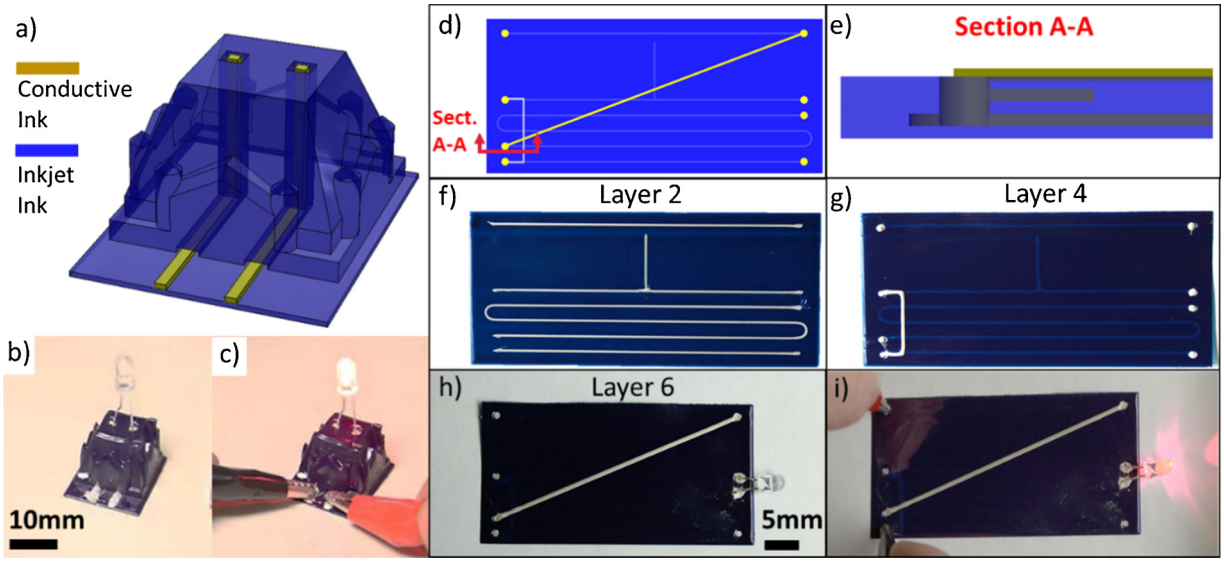

Fig. 7. a) Schematic of the Tech Tower VIA. b) As-printed VIA with LED placed into vertical circuit lines. c) LED illuminated after applying power demonstrating minimal voltage drop across vertical circuit lines. d) Schematic of the 6-layer PWB utilizing VIAs to connect multiple layers. e) A cross-section schematic showing the multiple layers of the VIA-based PWB. f) Layer 2. g) Layer 4. h) Layer 6 with an LED attached to transmission lines 2 and 3. i) LED light illuminated after providing power to lines 1 and 4.

sintered by placing the sample in an oven at 80 °C after printing. The final VIA height was measured to be 15 mm and the as-printed structure can be seen in Fig. 7b. To test the VIA circuit, an LED light was placed into the vertical connections and a power source was connected to the horizontal wires. As seen in Fig. 7c, the LED illuminates using 2 V demonstrating minimal voltage drop across the vertical lines. The overall end-to-end resistance of the VIA was measured to be 40 Ohms. The total time required to fabricate the VIA-based circuit shown here was approximately 30 min, greatly reducing the time needed using traditional approaches.

3.3.3. VIA-based printed wiring board

Printed wiring boards (PWBs) are widely used in modern electronics and typically involve multiple layers of matrix material as well as complex circuitry. Here, we demonstrate the capability of printing a six layer PWB using the m^4 printer (Fig. 7). Here, four distinct conductive traces, resembling radio transmission lines, were printed on the second layer. To connect these conductive lines, however, VIAs would be needed to provide a vertical connection to another layer of the PWB as the conductive traces could not pass over one another. In the next layer the inkjet was used to cover the traces with holes for the vertical VIAs. On the fourth layer, traces 1 and 3 were connected followed by an inkjet layer to cover the connecting trace. On the sixth layer conductive traces 2 and 4 were connected with a diagonal line. To demonstrate the connectivity of the circuitry an LED light was connected to lines 2 and 3. Power was then provided to lines 1 and 4 to illuminate the LED as seen in Fig. 7i.

3.4. Using PnP to fabricate a digital LED light

By integrating robotics into the m^4 printer, PnP operations can be performed allowing for the incorporation of pre-fabricated electronic components within a 3D printed structure. Here a digital LED lamp was fabricated by printing a base structure with FFF. The base structure was a PLA rectangle with a hollow pocket for the 50 W LED and connecting channels for the printed silver electrodes. Fig. 8a and b show a cross section schematic and a CAD rendering of the printed part with the three components, the PLA structure, silver electrode wires and the LED chip. Screenshot images of the printing process are shown in Fig. 8c–j with the full video shown in the SM (video 4). The PLA structure was first FFF printed exposing channels for the silver ink and a pocket for the LED chip (Fig. 8c). Next, the printing platform moved to the PnP location where the 6-axis robotic arm performed a pick (Fig. 8d) and place (Fig. 8e) operation to place the LED chip into the PLA structure. The printing platform then moved back to the extrusion module and conductive silver ink was DIW printed into the channels to provide connections to the LED from an external power supply (Fig. 8f). In previous demonstrations the silver conductive ink has been printed on flat substrates achieving good conductivity and material adhesion. Printing conductive ink on a rough FFF substrate, however, presented a challenge as silver would fall into the cracks between the individual traces of the PLA material ultimately decreasing or eliminating all silver conductivity. To mitigate this issue, multiple layers of conductive ink were deposited to ensure trace conductivity after all cracks had been filled. The Xenon photonic curing module was then used to cure the conductive silver ink to a resistance of approximately 10 Ω. Finally, the LED was encapsulated in PLA using the FFF printhead (Fig. 8g–h). After the part was printed, external wires were inserted into the channels containing the printed silver electrodes to provide connections to an external power supply (Fig. 8i). Turning on the power supply and providing power illuminated the LED as seen in Fig. 8j. The brightness of the digital LED could be tuned by adjusting the supplied current. The voltage supplied was 3 V with a maximum applied current of 1.5 A.

3.5. Discussions

While the primary goal of this paper is to establish a new multi-material multi-method 3D printing platform, our work also reveals some challenges, many of which should be addressed by the AM community. The following discussions seek to detail these challenges, explore possible solutions, and give a future perspective.

Currently, a design software that can automatically determine the proper methods and materials to use when printing a complex, multi-material structure does not exist. For example, existing 3D design software packages such as AutoCAD or Solidworks cannot determine which portion of a 3D printed object should be conductive, soft, or rigid depending on the desired application. In this work, separate 3D design files were generated for each material and combined in Repetier; G-code generating software. Repetier allows users to select tools that can be used to print each material, or 3D design file. Some efforts have been

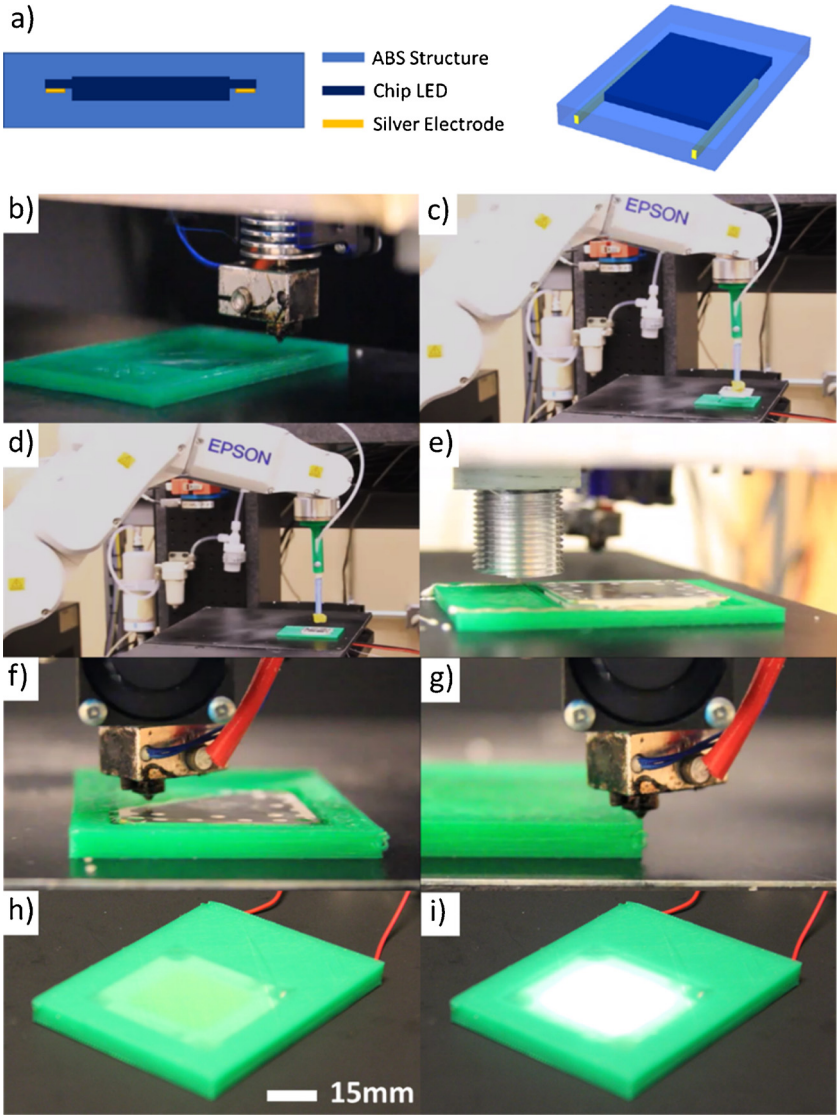

Fig. 8. Hybrid printing process of the digital LED. (a) Schematic of the digital LED light with a cross-section showing the three components and (b) an isometric view. (c) FFF printing of the flashlight case. (d) 6-axis Epson robot performing a pick and (e) place operation of the LED light. (d) DIW printing of conductive silver lines. (g–h) encapsulation of LED with further FFF layers, and (i) the final printed LED light. (j) Final printed flashlight and demonstration of functionality when connected to a power source.

made by Autodesk via project Cyborg, a tool that can help predict how to place multiple materials in 3D space depending on the desired application [49]. This method, however, still lacks the ability to predict how to use various printing methodologies. For example, when designing structures which use various printing methods, the output layer thickness or curing mechanisms may change between methods. Thus, a specific sequence of printing and curing motions must be generated based on the selected materials and methods. Therefore, further advancements from a software development standpoint must be made to further progress the field of multi-material multi-method 3D printing.

When designing inks to use with the m^4 3D printer, it became clear that material bonding will be a primary challenge that must be overcome. Therefore, in this work, we utilized materials that had similar curing characteristics to promote chemical bonding. The elastomer and inkjet materials are both acrylate-based polymers which utilize photo-crosslinking reactions after 3D printing. Through material diffusion prior to crosslinking, chemical bonding between the acrylate groups was achieved [29,50]. Microscope images of some multi-material interfaces can be found in Fig. S3 in the SM. In the future, further solutions must be developed to generate bonding methods between materials with a wide array of chemical structures and curing mechanisms.

Directly after 3D printing, many materials require curing via an energy source such as heat or UV exposure. During the curing process these materials experience volume shrinkage or expansion and every material experiences a different amount of volume shrinkage [51]. When printing a range of materials in the same object, a mismatch in shrinkage strain may develop, causing warping, bending, or other defects. In this study, to mitigate these effects, materials with minimal shrinkage strains upon curing were used. In addition, each multi-material layer was printed and cured before the next was deposited, limiting large shrinkage strain mismatch between different materials. Some researchers have developed models to better understand and therefore eliminate the unwanted effect of volume shrinkage [51–53]. In the future, novel printing strategies, or materials must be developed to solve the issues associated with volume shrinkage mismatch between multiple materials during curing.

For pick-and-place, or PnP, proper part orientation is a common challenge encountered while performing the operations. In this paper, before performing all PnP operations, the parts were oriented so that

they would be properly placed within the printed part. The robot was also programmed to pick up and place the part in a specific manner to further ensure proper orientation of the part prior to printing. In the future, fiducial markers, or markers located in fixed positions on the 3D printing stage, can be used for machine vision-assisted PnP, which is an area of active research in our group.

Another challenge encountered when using multiple printing methods is the resulting difference in resolution, such as layer thicknesses, between different methods. This presents a potential downside of integrating multiple methodologies because if a single printing method is used, the feature size depends on the resolution of that method. When multiple methods are used, however, the feature size depends on the methodology with the lowest resolution. In addition, the difference in layer thickness must be accounted for with each unique combination of methodologies. In this work, due to the difference in layer thickness encountered between DIW and IJ printing, eight layers of IJ material were deposited for every layer of DIW material, as previously determined by Li, et al. [43], where the thickness of each layer was measured after printing to ensure layer height matching between different printing approaches. This approach was used for all combinations of materials throughout this work.

Regarding conductivity on various substrates, in general, the conductivity of printed conductive inks depends not only on the ink's properties, but also on the substrate's surface properties, such as surface roughness. For example, in previous demonstrations, the silver conductive ink has been printed on flat substrates achieving good conductivity and material adhesion [40]. However, we found that printing conductive ink on a rough FFF substrate presented a challenge as silver would fall into the cracks between the individual traces of the PLA material, ultimately decreasing or eliminating silver conductivity. More comprehensive studies on how substrate properties can affect the resulting trace conductivity should be investigated.

4. Conclusion

The hybrid manufacturing platform presented within this manuscript demonstrates a highly integrated multi-material multi-method, or m^4, platform laying the groundwork for the future of 3D printable components. Here, complex objects, previously unobtainable using conventional 3D printing methodologies were presented. In addition, objects were manufactured in a time-efficient, single-platform design, in contrast to current manufacturing strategies that rely on multiple manufacturing techniques. The m^4 3D printer has demonstrated an enormous design space for mechanically heterogenous structures that could be integrated with pre-fabricated components and technologies. This technology exhibits a promising tool for research within the fields of mechanics, materials science, medicine, and biology.

Declaration of Competing Interest

The authors declare no conflict of interest.

Acknowledgements

The supports of an AFOSR grant (FA9550-16-1-0160; Dr. B.-L. "Les" Lee, Program Manager) and an AFOSR DURIP grant (FA9550-16-1-0169) are gratefully acknowledged. Gift funds from HP, Inc and Northrop Grumman Corporation are also greatly appreciated.

Appendix A. Supplementary data

Supplementary material related to this article can be found, in the online version, at doi:https://doi.org/10.1016/j.addma.2019.100819.

References

[1] Hull, C.W., Apparatus for production of three-dimensional objects by stereolithography. 1986, Google Patents.
[2] B. Kianian, Wohlers Report 2017: 3D Printing and Additive Manufacturing State of the Industry, Annual Worldwide Progress Report: Chapters Titles: The Middle East, and Other Countries, (2017).
[3] marketsandmarkets.com, 3D Printing Market by Offering (Printer, Material, Software, Service), Process (Binder Jetting, Direct Energy Deposition, Material Extrusion, Material Jetting, Powder Bed Fusion), Application, Vertical, and Geography - Global Forecast to 2023. marketsandmarkets.cOm, (2017).
[4] L. Columbus, The State of 3D Printing, 2017. Forbes.com, (2017).
[5] S. Ridinger, NASA Advances Additive Manufacturing For Rocket Propulsion. nasa.gov, (2017).
[6] R. Aston, 3D Printing Done Right: Applying Additive Manufacturing in Integrated Mechanical Designs. boeing.cOm, (2017).
[7] L.E. Murr, E. Martinez, K.N. Amato, S.M. Gaytan, J. Hernandez, D.A. Ramirez, P.W. Shindo, F. Medina, R.B. Wicker, Fabrication of metal and alloy components by additive manufacturing: examples of 3D materials science, J. Mater. Res. Technol. 1 (1) (2012) 42–54.
[8] Q. Zhang, D.J. Roach, L. Geng, H. Chen, H.J. Qi, D. Fang, Highly stretchable and conductive fibers enabled by liquid metal dip-coating, Smart Mater. Struct. 27 (3) (2018) 035019.
[9] W.E. Frazier, Metal additive manufacturing: a review, J. Mater. Eng. Perform. 23 (6) (2014) 1917–1928.
[10] Q. Mu, L. Wang, C.K. Dunn, X. Kuang, F. Duan, Z. Zhang, H.J. Qi, T. Wang, Digital light processing 3D printing of conductive complex structures, Addit. Manuf. 18 (2017) 74–83.
[11] M. Quanyi, K.D. Conner, W. Lei, L.D. Martin, H.J. Qi, W. Tiejun, Thermal cure effects on electromechanical properties of conductive wires by direct ink write for 4D printing and soft machines, Smart Mater. Struct. 26 (4) (2017) 045008.
[12] E. Macdonald, R. Salas, D. Espalin, M. Perez, E. Aguilera, D. Muse, R.B. Wicker, 3D printing for the rapid prototyping of structural electronics, IEEE Access 2 (2014) 234–242.
[13] D. Espalin, D.W. Muse, E. MacDonald, R.B. Wicker, 3D Printing multifunctionality: structures with electronics, Int. J. Adv. Manuf. Technol. 72 (5) (2014) 963–978.
[14] Z.X. Khoo, J.E.M. Teoh, Y. Liu, C.K. Chua, S. Yang, J. An, K.F. Leong, W.Y. Yeong, 3D printing of smart materials: a review on recent progresses in 4D printing, Virtual Phys. Prototyp. 10 (3) (2015) 103–122.
[15] Q. Ge, K.D. Conner, H.J. Qi, L.D. Martin, Active origami by 4D printing, Smart Mater. Struct. 23 (9) (2014) 094007.
[16] Q. Ge, H.J. Qi, M.L. Dunn, Active materials by four-dimension printing, Appl. Phys. Lett. 103 (13) (2013) 131901.
[17] K. Yu, A. Ritchie, Y. Mao, M.L. Dunn, H.J. Qi, Controlled sequential shape changing components by 3D printing of shape memory polymer multimaterials, Procedia IUTAM 12 (2015) 193–203.
[18] D.J. Roach, C. Hamel, J. Wu, X. Kuang, M.L. Dunn, H.J. Qi, 4-D Printing: Potential Applications of 3-D Printed Active Composite Materials Vol. 4 Homeland Defense and Security Information Analysis Center, 2017 4.
[19] Z.C. Eckel, C. Zhou, J.H. Martin, A.J. Jacobsen, W.B. Carter, T.A. Schaedler, Additive manufacturing of polymer-derived ceramics, Science 351 (6268) (2016) 58–62.
[20] U. Scheithauer, E. Schwarzer, H.-J. Richter, T. Moritz, Thermoplastic 3D printing—an additive manufacturing method for producing dense ceramics, Int. J. Appl. Ceram. Technol. 12 (1) (2015) 26–31.
[21] A. Zocca, P. Colombo, C.M. Gomes, J. Günster, Additive manufacturing of ceramics: issues, potentialities, and opportunities, J. Am. Ceram. Soc. 98 (7) (2015) 1983–2001.
[22] A. F2792-12a, Standard Terminology for Additive Manufacturing Technologies, (2019).
[23] Y.-F. Zhang, N. Zhang, H. Hingorani, N. Ding, D. Wang, C. Yuan, B. Zhang, G. Gu, Q. Ge, Fast-response, stiffness-tunable soft actuator by hybrid multimaterial 3D printing, Adv. Funct. Mater. (2019) 1806698 **0**(0).
[24] C. Yuan, D.J. Roach, C.K. Dunn, Q. Mu, X. Kuang, C.M. Yakacki, T.J. Wang, K. Yu, H.J. Qi, 3D printed reversible shape changing soft actuators assisted by liquid crystal elastomers, Soft Matter 13 (33) (2017) 5558–5568.
[25] D.J.K. Roach, Xiao, Chao Yuan, Kaijuen Chen, H. Qi, Jerry, Novel ink for ambient condition printing of liquid crystal elastomers for 4D printing, Smart Mater. Struct. (2018) [Accepted].
[26] E. Lin, Y. Li, C. Ortiz, M.C. Boyce, 3D printed, bio-inspired prototypes and analytical models for structured suture interfaces with geometrically-tuned deformation and failure behavior, J. Mech. Phys. Solids 73 (2014) 166–182.
[27] G.X. Gu, M. Takaffoli, M.J. Buehler, Hierarchically enhanced impact resistance of bioinspired composites, Adv. Mater. 29 (28) (2017) 1700060.
[28] R. Mirzaeifar, L.S. Dimas, Z. Qin, M.J. Buehler, Defect-tolerant bioinspired hierarchical composites: simulation and experiment, ACS Biomater. Sci. Eng. 1 (5) (2015) 295–304.
[29] Z. Ding, C. Yuan, X. Peng, T. Wang, H.J. Qi, M.L. Dunn, Direct 4D printing via active composite materials, Sci. Adv. 3 (4) (2017).
[30] J. Wu, C. Yuan, Z. Ding, M. Isakov, Y. Mao, T. Wang, M.L. Dunn, H.J. Qi, Multi-shape active composites by 3D printing of digital shape memory polymers, Sci. Rep. 6 (2016) 24224.
[31] E. David, A.R. Jorge, M. Francisco, W. Ryan, Multi-material, multi-technology FDM: exploring build process variations, Rapid Prototyp. J. 20 (3) (2014) 236–244.
[32] J.-W. Choi, E. MacDonald, R. Wicker, Multi-material microstereolithography, Int. J.

Adv. Manuf. Technol. 49 (5) (2010) 543–551.
[33] Y. Pan, C. Zhou, Y. Chen, A fast mask projection stereolithography process for fabricating digital models in minutes, J. Manuf. Sci. Eng. 134 (5) (2012) p. 051011-051011-9.
[34] J.L. Amit, M. Eric, W.R. B, Integrating stereolithography and direct print technologies for 3D structural electronics fabrication, Rapid Prototyp. J. 18 (2) (2012) 129–143.
[35] E. MacDonald, R. Wicker, Multiprocess 3D printing for increasing component functionality, Science 353 (6307) (2016).
[36] N.A. Meisel, A.M. Elliott, C.B. Williams, A procedure for creating actuated joints via embedding shape memory alloys in PolyJet 3D printing, J. Intell. Mater. Syst. Struct. 26 (12) (2015) 1498–1512.
[37] K.B. Perez, C.B. Williams, Design considerations for hybridizing additive manufacturing and direct write technologies, Proceedings of the Asme International Design Engineering Technical Conferences and Computers and Information in Engineering Conference, 2014 Vol 4 (2014).
[38] G.W. Wagner, L.B. Bass, D.A. Rau, S.B. Ziv, M.S. Wolf, D.L. Wolf, Y. Bai, V. Meenakshisundaram, C.B. Williams, Design and development of a multi-tool additive manufacturing system, The 28th Annual International Solid Freeform Fabrication Symposium (2017).
[39] J.T. Muth, D.M. Vogt, R.L. Truby, Y. Mengüç, D.B. Kolesky, R.J. Wood, J.A. Lewis, Embedded 3D printing of strain sensors within highly stretchable elastomers, Adv. Mater. 26 (36) (2014) 6307–6312.
[40] Q. Mu, M. Lei, D.J. Roach, C.K. Dunn, X. Kuang, C. Yuan, T. Wang, H.J. Qi, Intense pulsed light sintering of thick conductive wires on elastomeric dark substrate for hybrid 3D printing applications, Smart Mater. Struct. 27 (11) (2018) 115007.
[41] X. Kuang, K. Chen, C.K. Dunn, J. Wu, V.C.F. Li, H.J. Qi, 3D printing of highly stretchable, shape-memory and self-healing elastomer toward novel 4D printing, ACS Appl. Mater. Interfaces 10 (8) (2018) 7381–7388.
[42] D.J. Roach, X. Kuang, C. Yuan, K.J. Chen, H.J. Qi, Novel ink for ambient condition printing of liquid crystal elastomers for 4D printing, Smart Mater. Struct. 27 (12) (2018).
[43] V.C.-F. Li, X. Kuang, C.M. Hamel, D. Roach, Y. Deng, H.J. Qi, Cellulose nanocrystals support material for 3D printing complexly shaped structures via multi-materials-multi-methods printing, Addit. Manuf. 28 (2019) 14–22.
[44] C. Laschi, B. Mazzolai, M. Cianchetti, Soft robotics: technologies and systems pushing the boundaries of robot abilities, Sci. Robot. 1 (1) (2016).
[45] D. Trivedi, C.D. Rahn, W.M. Kier, I.D. Walker, Soft robotics: biological inspiration, state of the art, and future research, Appl. Bionics Biomech. 5 (3) (2008) 99–117.
[46] R.F. Shepherd, F. Ilievski, W. Choi, S.A. Morin, A.A. Stokes, A.D. Mazzeo, X. Chen, M. Wang, G.M. Whitesides, Multigait soft robot, Proc. Natl. Acad. Sci. 108 (51) (2011) 20400–20403.
[47] B. Mosadegh, P. Polygerinos, C. Keplinger, S. Wennstedt, R.F. Shepherd, U. Gupta, J. Shim, K. Bertoldi, C.J. Walsh, G.M. Whitesides, Pneumatic networks for Soft robotics that actuate rapidly, Adv. Funct. Mater. 24 (15) (2014) 2163–2170.
[48] L, V.J, A. Katzenmeyer, M.S. Islam, N.P. Kobayashi, W. Wu, P. Chaturvedi, N.X. Fang, S.Y. Wang, R.S. Williams, Electrical resistivity & thermal stability of smooth silver thin film for nanoscale optoelectronic devices, 2008 8th IEEE Conference on Nanotechnology, (2008).
[49] S. Miyashita, I. DiDio, I. Ananthabhotla, B. An, C. Sung, S. Arabagi, D. Rus, Folding angle regulation by curved crease design for self-assembling origami propellers, J. Mech. Robot. 7 (2) (2015) p. 021013-021013-8.
[50] S. Sundaram, D.S. Kim, M.A. Baldo, R.C. Hayward, W. Matusik, 3D-printed self-folding electronics, ACS Appl. Mater. Interfaces 9 (37) (2017) 32290–32298.
[51] J. Wu, Z. Zhao, C.M. Hamel, X. Mu, X. Kuang, Z. Guo, H.J. Qi, Evolution of material properties during free radical photopolymerization, J. Mech. Phys. Solids 112 (2018) 25–49.
[52] Q. Huang, J. Zhang, A. Sabbaghi, T. Dasgupta, Optimal offline compensation of shape shrinkage for three-dimensional printing processes, IIE Trans. 47 (5) (2015) 431–441.
[53] B. Lu, P. Xiao, M. Sun, J. Nie, Reducing volume shrinkage by low-temperature photopolymerization, J. Appl. Polym. Sci. 104 (2) (2007) 1126–1130.